NASA Technical Memorandum 4417

Correlation of Forebody Pressures and Aircraft Yawing Moments on the X-29A Aircraft at High Angles of Attack

David F. Fisher
Dryden Flight Research Facility
Edwards, California

David M. Richwine and Stephen Landers
PRC Inc.
Edwards, California

National Aeronautics a
Space Administration
Office of Management
Scientific and Technica
Information Program
1992

(NASA-TM-4417) CORRELATION OF FOREBODY PRESSURES AND AIRCRAFT YAWING MOMENTS ON THE X-29A AIRCRAFT AT HIGH ANGLES OF ATTACK (NASA) 17 p

N93-11532

Unclas

H1/02 0126296

CORRELATION OF FOREBODY PRESSURES AND AIRCRAFT YAWING MOMENTS ON THE X-29A AIRCRAFT AT HIGH ANGLES OF ATTACK

David F. Fisher*
NASA Dryden Flight Research Facility
P.O. Box 273
Edwards, California 93523-0273

David M. Richwine** and Stephen Landers†
PRC Inc.
P.O. Box 273
Edwards, California 93523-0273

Abstract

In-flight pressure distributions at four fuselage stations on the forebody of the X-29A aircraft have been reported at angles of attack from 15 to 66° and at Mach numbers from 0.22 to 0.60. At angles of attack of 20° and higher, vortices shed from the nose strake caused suction peaks in the pressure distributions that generally increased in magnitude with angle of attack. Above 30°-angle of attack, the forebody pressure distributions became asymmetrical at the most forward station, while they remained nearly symmetrical until 50- to 55°-angle of attack for the aft stations. Between 59- to 66°-angle of attack, the asymmetry of the pressure distributions changed direction. Yawing moments for the forebody alone were obtained by integrating the forebody pressure distributions. At 45°-angle of attack, the aircraft yaws to the right and at 50° and higher, the aircraft yaws to the left. The forebody yawing moments correlated well with the aircraft left yawing moment at an angle of attack of 50° or higher. At a 45°-angle of attack, the forebody yawing moments did not correlate well with the aircraft yawing moment, but it is suggested that this was due to asymmetric pressures on the cockpit region of the fuselage which was not instrumented. The forebody was also shown to provide a positive component of directional stability of the aircraft at angles of attack of 25° or higher. A Mach number effect was noted at angles of attack of 30° or higher at the station where the nose strake was present. At this station, the suction peaks in the pressure distributions at the highest Mach number were reduced and much more symmetrical as compared to the lower Mach number pressure distributions.

Nomenclature

C_p	pressure coefficient
C_n	yawing moment coefficient
C_{nfb}	forebody yawing moment coefficient determined from integration of forebody pressures over projected side area
C_{n_0}	yawing moment coefficient at zero sideslip
$C_{n_{0,fb}}$	forebody yawing moment coefficient at zero sideslip, $\beta = 0$ intercept of C_{nfb} versus β curve
$C_n\beta$	aircraft directional stability
$C_n\beta_{,fb}$	forebody directional stability coefficient, $\frac{\partial C_{nfb}}{\partial \beta}$, deg^{-1}
F.S.	fuselage station, in.
HARV	High Alpha Research Vehicle
l	length of aircraft from nose apex to engine exhaust plane, 576 in.
M	Mach number
Re_c	Reynolds number based on mean aerodynamic chord of 86.60 in.
Re_D	Reynolds number based on fuselage major axis diameter of 39.8 in. at x/l = 0.201
x	distance from nose apex along longitudinal axis of aircraft
α	aircraft angle of attack, deg
β	aircraft angle of sideslip, deg

*Aerospace engineer. Member AIAA.
**Aerospace engineer. Member AIAA.
†Aerospace engineer.

Copyright ©1992 by the American Institute of Aeronautics and Astronautics, Inc. No copyright is asserted in the United States under Title 17, U.S. Code. The U.S. Government has a royalty-free license to exercise all rights under the copyright claimed herein for Governmental purposes. All other rights are reserved by the copyright owner.

θ forebody circumferential angle, deg, (0° is bottom centerline, positive is clockwise as seen from a front view, 0 to 360°)

Introduction

A joint high-angle-of-attack research program on the forward-swept-wing close-coupled canard X-29A airplane (Fig. 1) was recently completed by NASA, the U.S. Air Force, and Grumman. This program studied flight controls, handling qualities, fighter agility–military utility, flow visualization, and forebody pressure measurements.

During the high-angle-of-attack envelope expansion and subsequent flight testing of the X-29A, the aircraft generally exhibited excellent slow-speed flying qualities at high angles of attack. The purpose of those flights was to evaluate the aircraft in full maneuvering flight up to 40°-angle of attack (α) and during symmetric pullups or pitch pointing to $\alpha = 70°$. At $\alpha \approx 45°$, an interesting phenomenon appeared in which the aircraft always yawed to the right. If full opposite rudder was input prior to the buildup of yaw rate, lateral control could be maintained using conventional lateral stick inputs. At $\alpha \geq 50°$, the aircraft yawed to the left and no piloting technique was sufficient to maintain a constant heading at 30,000-ft altitude and above.[1]

The X-29A had been designed to be departure resistant throughout the flight envelope, including the high-angle-of-attack region.[2] The Grumman design incorporated existing aircraft hardware to reduce development costs. This included an F-5A nose section which was known to have forebody-induced yaw asymmetries at high angles of attack and was modified because of this asymmetry.

With the original F-5A forebody shape, the nose asymmetry phenomenon was characterized by large sideforces at 0° sideslip (β) above $\alpha = 23°$. This forebody shape was modified for the X-29A application through a series of wind-tunnel tests.[3] Both nose strakes and an F-20 shark nose[4] configuration were tested in hope of alleviating the asymmetry. While the nose strakes and the shark nose eliminated the asymmetry at low Reynolds numbers, the shark nose data were not repeatable in high Reynolds number tests. The final X-29A nose shape consisted of a refinement of the nose strakes and shortening the F-5A nose cone 11 in. The wind-tunnel tests described in Ref. 3 predicted that these refinements would delay any nose asymmetry phenomenon to $\alpha \approx 40°$. Later ground tests from the wind-tunnel and drop model tests showed the possibility of zero sideslip yaw asymmetries at $\alpha > 40°$.[5,6]

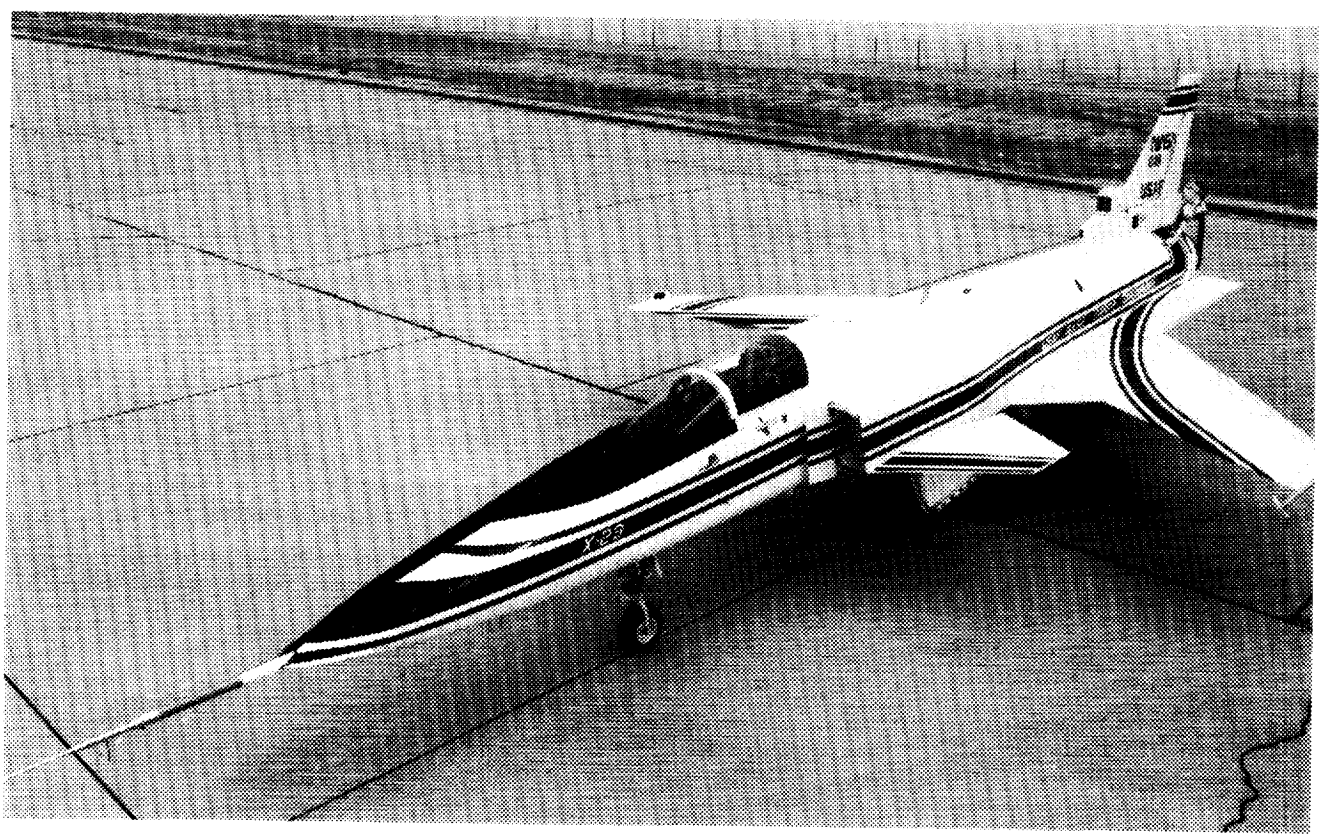

EC 91 517-21

Fig. 1 X-29 aircraft.

ORIGINAL PAGE
BLACK AND WHITE PHOTOGRAPH

The purpose of this flight test was to investigate the reasons for these nose asymmetries observed in flight and to gain a better understanding of vortical flows on forebodies at high angles of attack. Flow visualization and extensive surface pressure measurements on the forebody were to be used. Previously, similar instrumentation had been used on the F-18 High Alpha Research Vehicle (HARV)[7–9] to study vortical flow phenomena. In that case, off-surface flow visualization, on-surface flow visualization, and surface pressure measurements were used. As a result, locations of vortex cores, lines of separation, and laminar separation bubbles showed good correlation with the pressure distributions.

This X-29A study included smoke flow visualization and pressure distribution measurements. The off-surface flow visualization using smoke has been reported in Refs. 10 and 11. This paper summarizes the results of the forebody pressure measurements; preliminary results have been reported in Ref. 12. Pressure distributions will be presented and forebody yawing moments and directional stability derived from the integrated forebody pressures will be correlated with the aircraft yawing moments and directional stability.

Experiment Description

Vehicle Description

The X-29A is a single place research airplane which integrates several technologies, such as a forward-swept, aeroelastically tailored composite wing and a close-coupled, variable-incidence canard. The forward-swept wing section, with a 29.27° leading-edge swept wing, has a thin, supercritical wing with full span, dual-hinged flaperons and a fixed leading edge. An aft body strake flap augments the pitch control of the canard and the flaperons. Lateral control is provided by the full span asymmetrical deflection of the flaperon while a conventional rudder is used for directional control.

The Grumman design incorporated existing aircraft hardware to reduce development costs. This included a modified F-5A nose section; F-16 main gear, emergency power unit and surface actuators; F-14 flight sensors and Honeywell flight control computers; and an F-18 F-404-GE-400 afterburning turbofan engine (General Electric, Lynn, Massachusetts).

The original F-5A forebody had an unfavorable zero sideslip nose slice characteristic at high angles of attack.[13] To improve the high-angle-of-attack characteristics for the X-29A application, Grumman modified the forward 46 in. of the nose section by reshaping it, shortening it 11 in., and adding a 24-in. long nose strake. Figure 2 is a close-up view of the nose strake as seen from below. A noseboom 75-in. long was installed at the nose apex. The boom tapered from 0.88-in. diameter at the tip to 3.5-in. diameter at the nose apex and supported three angle-of-attack vanes and one angle-of-sideslip vane.

Instrumentation

For this investigation, the fuselage forward of the cockpit was extensively instrumented with surface pressure measurements as shown in Fig. 3. Four circumferential rows of static pressure orifices were installed at $x/l = 0.026$, 0.056, 0.136, and 0.201. A total of 202 orifices were installed. Gaps in the orifice installation at the circumferential rows were due to internal structure or lack of internal access. Each orifice on the forebody was connected to temperature-controlled electronic scanning pressure modules with 6 ft of 0.062-in. id pneumatic tubing. It was previously determined that 8 ft of 0.062 tubing would have a pneumatic lag of 10 msec at an altitude of 20,000 ft.[14] Reference pressure for the module was supplied through a 12-in. long, 0.062-in. id tubing to a small reference pressure manifold with an internal volume of 0.21 in^3 located in the forebody. The reference manifold, vented to the unpressurized compartment though an 8-in. long, 0.066-in. diameter tubing, was monitored by a high-resolution digital absolute pressure transducer. The pressure transducers with each module were scanned sequentially 25 samples/sec and outputs were sampled by a 10-bit pulse code modulation (PCM) data system. In-flight zero differential pressure readings were taken before each test point and were used during post-flight data reduction to correct the data for calibration offsets. The forebody pressures were measured with ± 216 lb/ft^2 differential range pressure transducers with an estimated accuracy of 1 lb/ft^2.

Airspeed and altitude were measured using a specially designed swivel probe which self aligned with the local flow and was mounted on the left wing tip (Fig. 4). This probe was calibrated for Mach number and altitude and its root-mean-square error was estimated to be 0.003 for $\alpha < 58°$ based on data from a similar installation on the F-18 HARV.[15] Since angle of attack was a flight-critical input parameter for the triple redundant flight-control system for this 35-percent statically unstable aircraft, three independent angle-of-attack vanes were mounted on the noseboom. For high angles of attack, the vanes were calibrated using the aircraft inertial navigation system and meterological analysis of rawinsonde ballon data.[16,17] A single vane mounted on the noseboom was used to determine angle of sideslip.

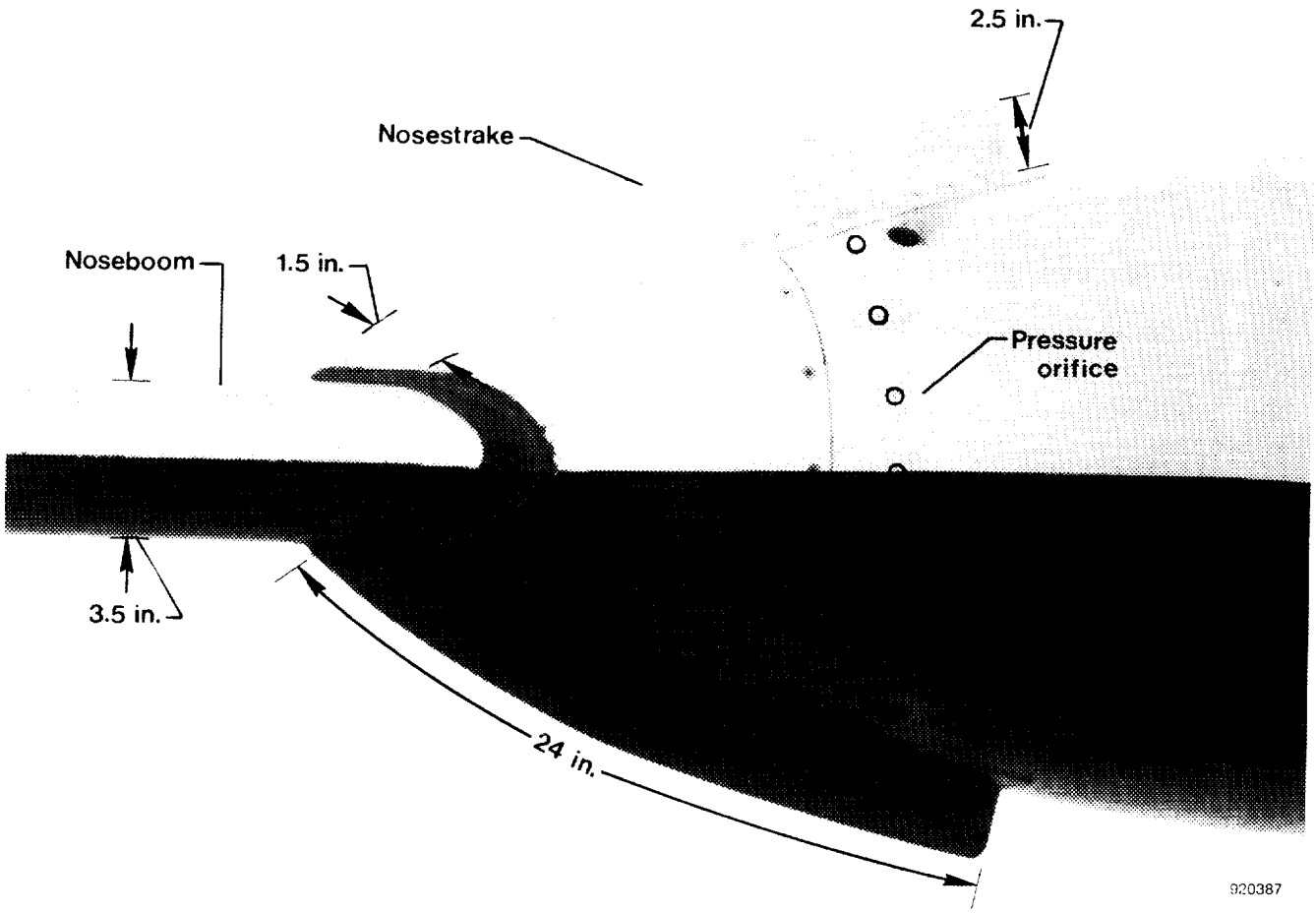

Fig. 2 X-29 aircraft.

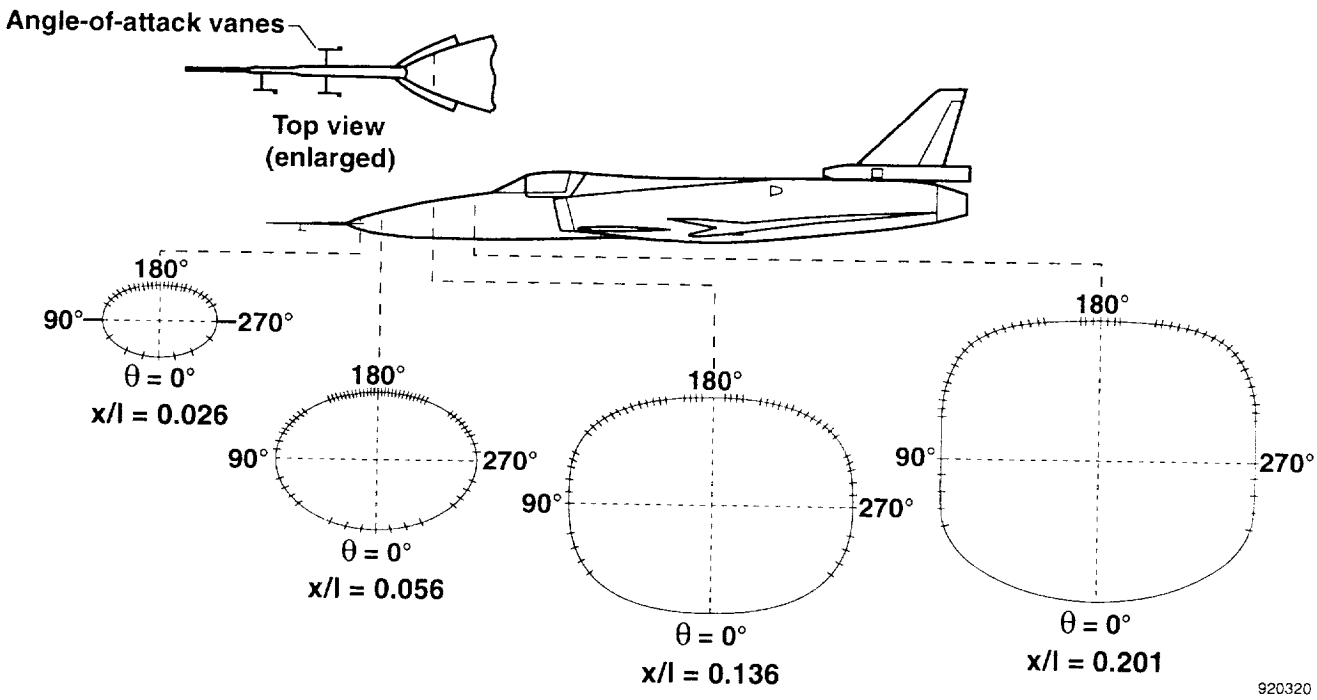

Fig. 3 Locations of pressure orifices on the X-29A forebody, cross sectional views from in front of aircraft.

ORIGINAL PAGE
BLACK AND WHITE PHOTOGRAPH

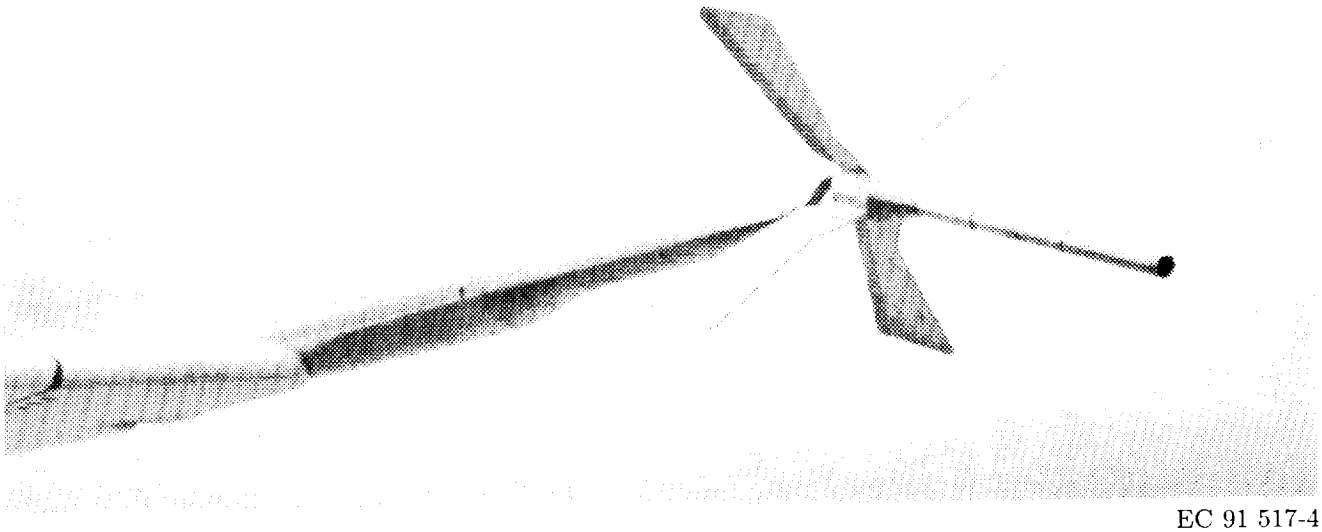

EC 91 517-4

Fig. 4 Swivel probe on left wing tip of the X-29A.

Test Conditions

Pressure distributions on the forebody were obtained at angles of attack from 15 to 50° during 1-g quasi-steady-state flight conditions, for zero and nonzero sideslip values at nominal altitudes of 20,000 and 40,000 ft. Sideslip data were obtained during controlled wings-level sideslip maneuvers for $\alpha \leq 45°$. At $\alpha \geq 45°$, sideslip data were obtained during wing rock and transient conditions during slow pullup–pushover maneuvers. Data were also obtained in windup turns at angles of attack from 15 to 40° for $M \leq 0.60$.

Pressure distributions at $\alpha > 55°$ were obtained on a single flight during a pullup–pushover maneuver of which 6.5 sec were at $\alpha \geq 50°$. As mentioned in the Instrumentation section, there was little lag in the pneumatic tubing between the orifice and the pressure transducer. Data from this dynamic maneuver at $\alpha \leq 55°$ were consistent with similar data from stabilized test points on other flights. The data from this dynamic maneuver at $\alpha > 55°$, while limited, are thought to be valid.

At $\alpha \leq 50°$, the flight data were averaged for 0.4 sec during quasi-steady-state conditions or slow, wings-level sideslip maneuvers, resulting in the average value for a total of 10 data samples. At $\alpha > 50°$, the data interval had to be reduced due to the more transient maneuvers, and data intervals of 0.1 and 0.2 sec were used.

Discussion of the Results

Effect of Angle of Attack

Forebody Pressure Distributions Sample pressure coefficient data from the forebody are plotted as a function of radial location (θ) in Fig. 5. Radial location $\theta = 0°$ is on the fuselage bottom centerline, $\theta = 180°$ is on the fuselage top centerline, $\theta = 90°$ and 270° are points on the fuselage surface, and the horizontal line which bisects the vertical axis as shown in the figure inset. The cross-section view is taken looking aft from in front of the aircraft. Radial location $\theta = 90°$ is on the starboard (pilot's right) side and $\theta = 270°$ is on the port side. Note that the pressure distribution at each angle of attack shown is offset from the previous by $\Delta C_p = 1.0$. The complete ordinate scale is shown for $\alpha = 66.2°$ only. The angle of attack corresponding to each pressure distribution is shown at the right of the figure. A more complete listing of the flight conditions is given in the following table. At $\alpha = 20°$ and above, the effect of the nose strake vortices are noted by a sharp suction peak in the pressure distributions at $\theta \approx 108°$ and 252° (Fig. 5(a)). These suction peaks generally increase in magnitude with angle of attack. The pressure distributions at x/l = 0.026 were nearly symmetrical up to $\alpha = 30°$. Above $\alpha = 30°$, the pressure distributions became asymmetric. The suction peak was greater on the port (pilot's left) side suggesting that the port forebody strake vortex was slightly closer to the surface and the starboard (pilot's right) vortex was farther from the surface. The asymmetry remained in this direction until between $\alpha = 59$ to 66°, where the asymmetry switched direction and the higher suction pressure was on the starboard side.

At x/l = 0.056 (Fig. 5(b)), four distinct suction peaks became discernible in the pressure distributions. At $\alpha = 45.2°$, for example, the peaks at $\theta \approx 90°$ and 270° are caused by the flow accelerating around the highly curved surface of the forebody at this station. Suction

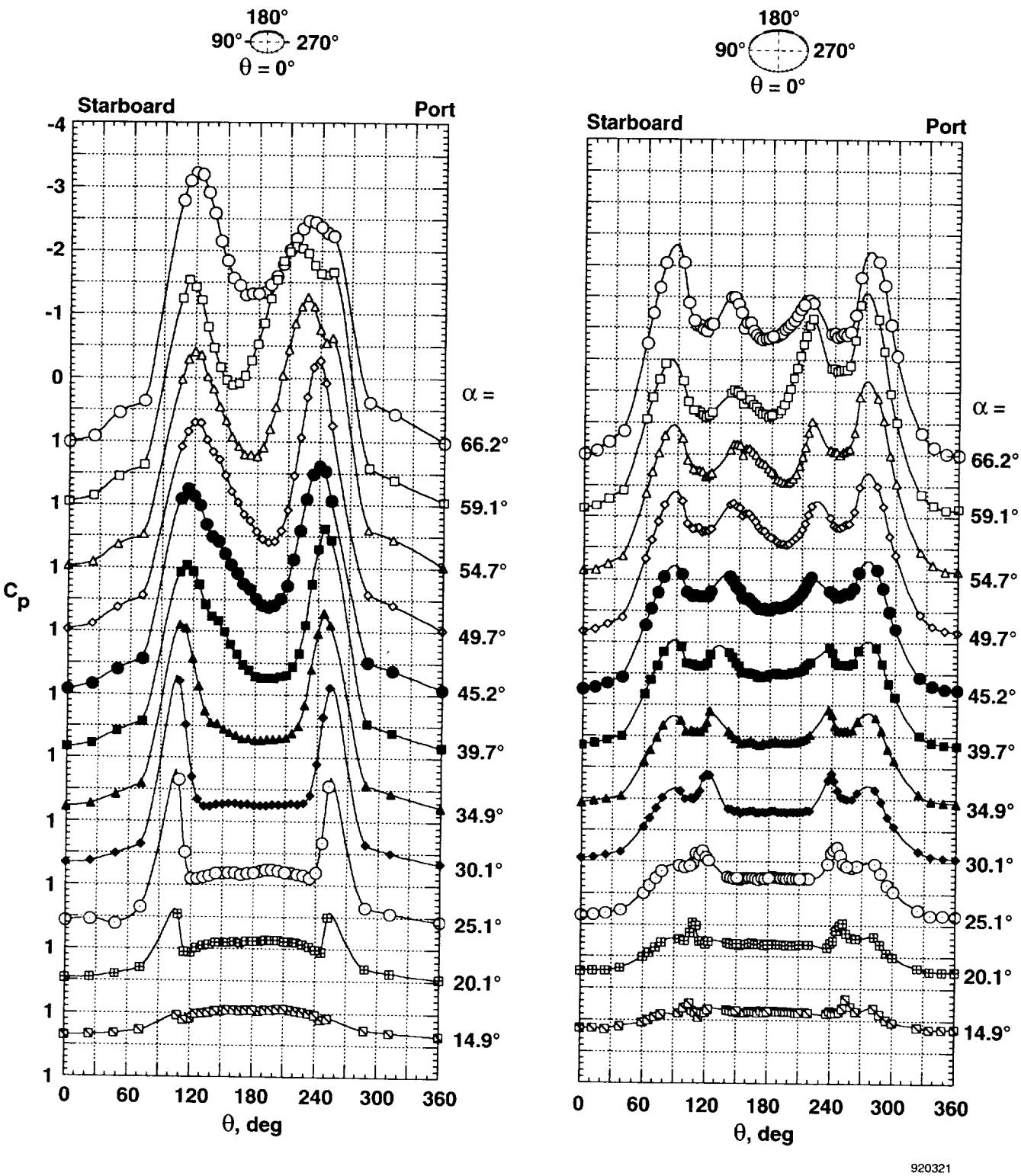

(a) x/l = 0.026.

(b) x/l = 0.056.

Fig. 5 Effect of angle of attack on forebody pressures.

peaks are also observed at $\theta \approx 140°$ and 220° at $\alpha = 45.2°$. These suction peaks are caused by the footprint of the nose strake vortices and are significantly reduced as compared to those at x/l = 0.026, suggesting that the nose strake vortices are farther from the surface at this location. As the angle of attack was increased from $\alpha = 14.9°$, these suction peaks moved inboard (toward $\theta = 180°$). Note that the pressure distribution does not become asymmetric until $\alpha = 49.7°$ with the higher suction pressures on the port side as it was for x/l = 0.026. At $\alpha = 66.2°$, the distribution has become nearly symmetric.

At x/l = 0.136, suction peaks in the pressure distribution shown in Fig. 5(c) at $\theta \approx 70°$ and 290° are caused by the local acceleration of the flow around the highly curved surface at these circumferential angles (Fig. 3). Suction peaks at $\theta \approx 160°$ and 200° for $\alpha = 45.2°$, for example, are due to the nose strake vortices and are reduced further compared to x/l = 0.056, suggesting a further lifting of the vortices from the surface. At this location the pressure distribution did not become significantly asymmetric until $\alpha = 54.7°$, with the higher suction pressures on the port side as seen previously at x/l = 0.026 and 0.056. At $\alpha = 66°$, the asymmetry changed direction with the high suction pressures on the starboard side as had happened at x/l = 0.026.

Moving farther aft on the forebody to x/l = 0.201 (Fig. 5(d)), the pressure distributions had suction peaks at $\theta \approx 60°$ and 300° due to the local acceleration about the highly curved surface at those radial locations. Minor suction peaks are noted near $\theta = 160°$ and 200° for $\alpha = 45.2°$ due to the further displaced nose strake vortices. The nose strake vortex at $\theta \approx 200°$, $\alpha = 49.7°$ and 54.7°, is closer to the surface and results in the increased suction. An additional suction peak is also noted in the pressure distribution and is distinct at $\alpha = 45.2°$ and $\theta = 250°$. This suction peak is probably due to the local acceleration of flow about the locally curved surface due to the proximity of the vortex on this side and resulting increased local velocities. Note that at $\alpha = 66.2°$, where the asymmetry has changed directions, this suction peak is more pronounced at $\theta = 110°$ than at 250°.

The data shown in Fig. 5 were obtained at a Reynolds number based on the fuselage diameter of $Re_D = 2.4$ to 3.9×10^6. These Reynolds numbers are above the critical Reynolds for ogive cylinders[18–20] and the boundary layer on the forebody should be turbulent. In addition, at x/l = 0.136 and 0.201, large removable panels for access to internal electronics cause a discontinuity in the surface just below the lowest orifice and would act as a boundary-layer trip if the flow were laminar.

Yawing Moments at Zero Sideslip Forebody yawing moment coefficients were determined by integrating the four rings of pressures over the projected forebody side area. The forebody yawing moment coefficient at zero sideslip ($C_{n_{0,fb}}$) was determined by plotting the forebody yawing moment coefficient (C_{nfb}) as a function of sideslip (β), fairing a line through the data, and obtaining the intercept at $\beta = 0$. Two examples of this procedure are shown in Fig. 6 at $\alpha \approx 45°$ and 55°. In Fig. 6(a), data at $\alpha \approx 45°$ are shown for altitudes of 20,000 and 40,000 ft as well as linear curve fit of this data. In Fig. 6(b), data at $\alpha \approx 55°$ are shown with the linear curve fit and error band. The equations for these linear curve fits give the offset ($C_{n_{0,fb}}$) as well as the slope ($C_{nfb\beta}$), i.e., the yawing moment at $\beta = 0$ and the directional stability parameter.

The yawing moment coefficients caused by the forebody and for the complete aircraft[21] are presented in Fig. 7 as a function of angle of attack. The complete aircraft data were taken at an altitude of 30,000 ft while the forebody data were taken near 20,000 ft and 40,000 ft. The large right aircraft yawing moment at zero sideslip at 45° did not correlate with the forebody pressures. There is, however, a strong correlation between the left yawing moment coefficient at $\alpha \geq 50°$. At $\alpha = 55°$ the forebody accounts for approximately 65 percent of the yawing moment. Above $\alpha = 60°$, the slope of the curve changes and $C_{n_{0,fb}} = 0$ at $\alpha \approx 65°$.

The forebody yawing moments at $\beta = 0$ were broken down further by individual orifice stations to determine which regions were causing the yawing moment. In Fig. 8, the yawing moments at $\beta = 0$ for a unit length (1 ft) of fuselage at each station are shown as a function of angle of attack. The effect for the orifice row at x/l = 0.026 is small partly because of its relatively small fuselage vertical height (minor diameter) and partly because of favorable effects of the nose strake.[19] At $\alpha \geq 55°$, the forebody stations at x/l = 0.056 and 0.136 have the most effect on the forebody yawing moment to the left. The forebody station at x/l = 0.201 has significantly less effect than either forebody station at x/l = 0.056 or 0.136 for $\alpha \geq 55°$. Note, however that at $\alpha = 45°$, the forebody station at x/l = 0.201 is showing a positive yawing moment while the yawing moment for the other stations is either nearly zero or slightly negative. This suggests that pressures on a forebody region aft of x/l = 0.201, possibly the canopy region, could be causing the nose-right yawing moments at $\alpha \approx 45°$. This is also in agreement with Ref. 22 which stated that "as the angle of attack (for an ogive cylinder) was increased, the side force distribution compressed toward the nose."

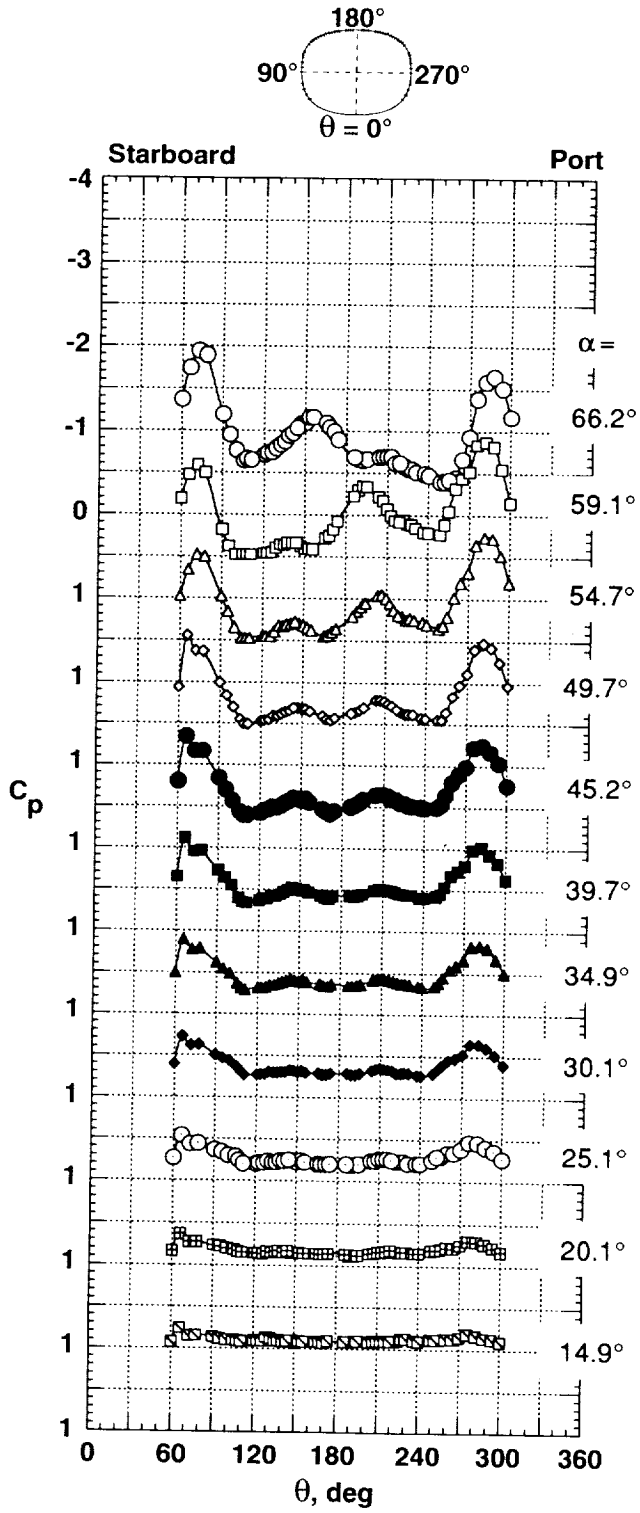

(c) x/l = 0.136.

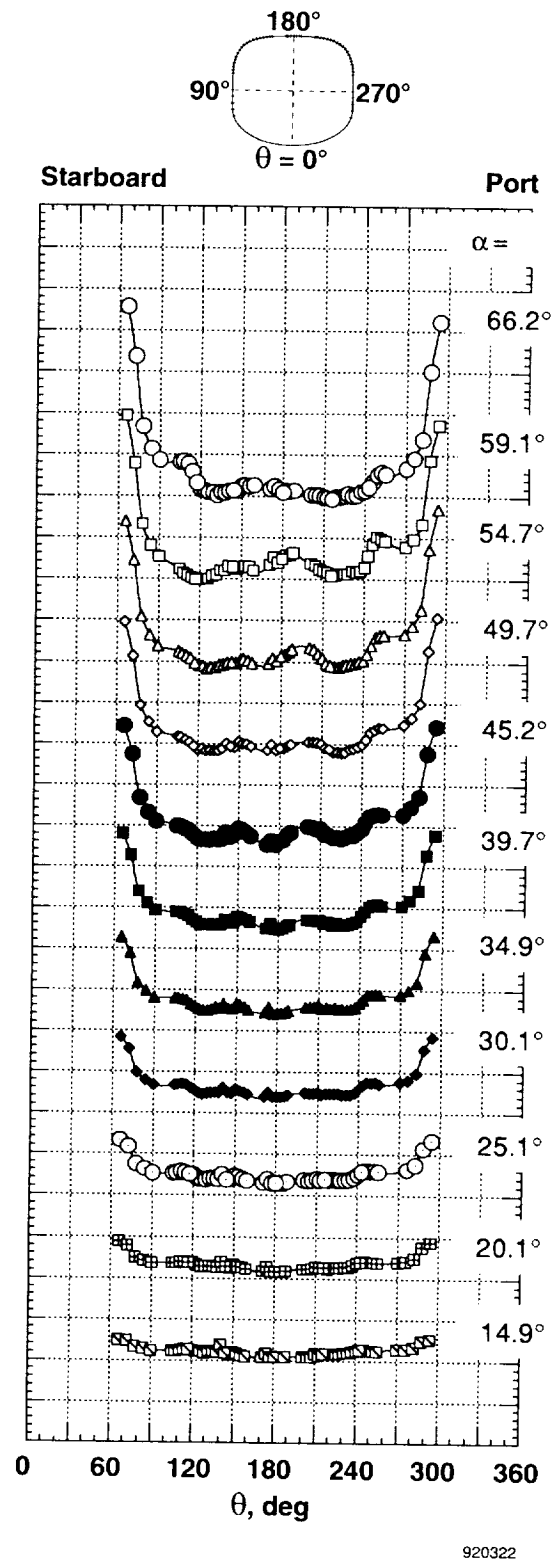

(d) x/l = 0.201.

Fig. 5 Concluded.

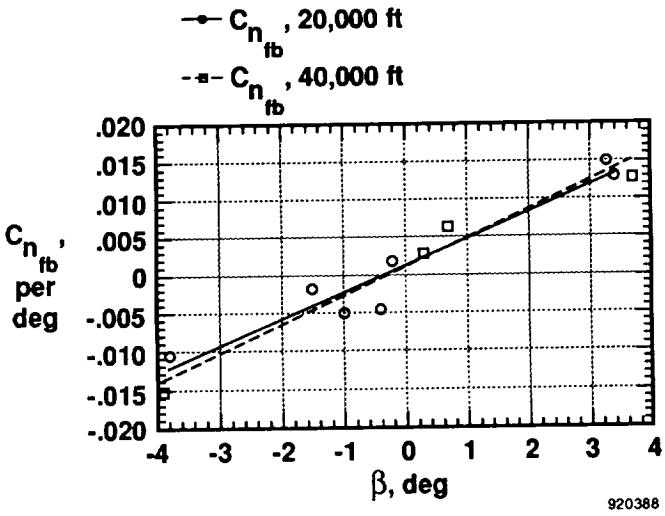

(a) $\alpha = 45°$.

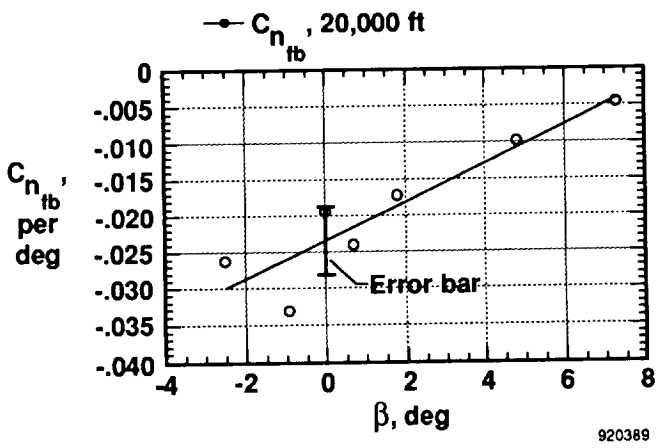

(b) $\alpha = 55°$.

Fig. 6 Forebody yawing moments as a function of sideslip.

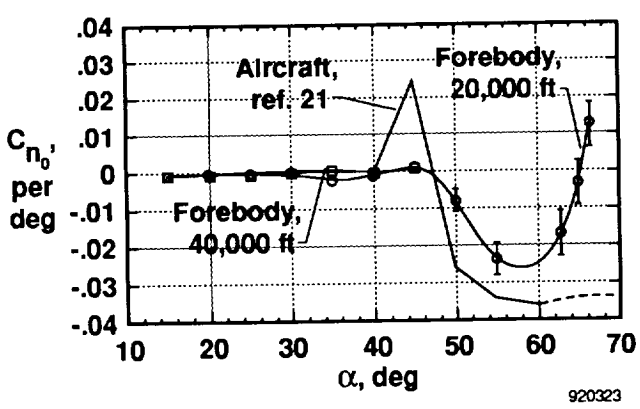

Fig. 7 Aircraft and forebody yawing moments at $\beta = 0°$.

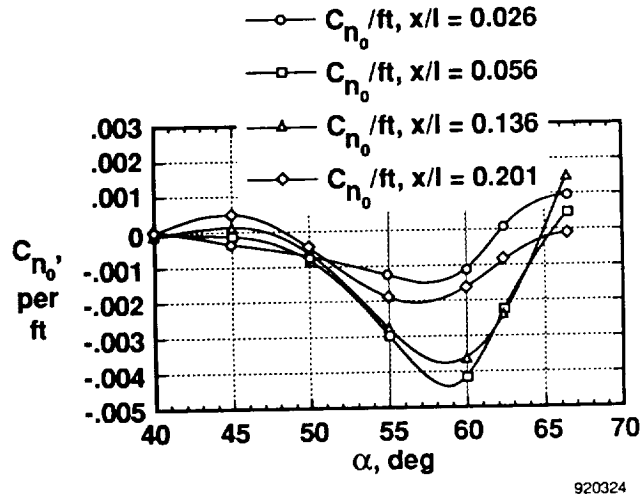

Fig. 8 Effect of angle of attack on forebody station yawing moment per unit length.

Effect of Angle of Sideslip

Directional Stability The contribution of the forebody to the aircraft directional stability ($C_{n_{fb}}\beta$) is shown in Fig. 9. Also shown in this figure is the total aircraft directional stability ($C_n\beta$) from Refs. 21 and 23 as well as the directional stability of an isolated F-5A forebody model as determined from force and moment data.[13] While the F-5A forebody model used was about 30 percent longer than the length used for the X-29A calculations, the moment centers as measured from the nose apex were nearly identical. At $\alpha \leq 25°$, the X-29A forebody shows increasing directional stability though not as much as the F-5A forebody, even accounting for the additional length. A significant portion of the directional stability of the X-29A at $\alpha > 35°$ can be attributed to the forebody.

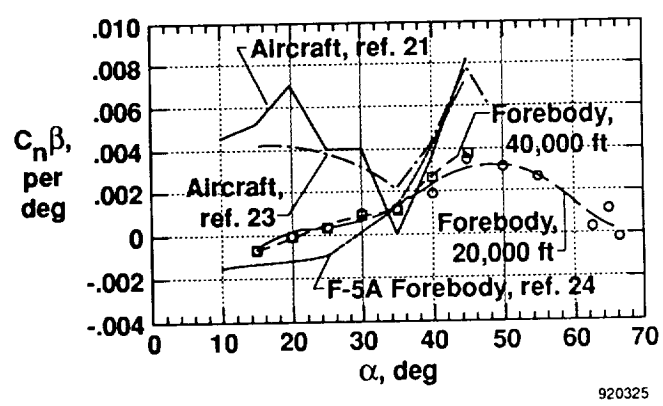

Fig. 9 X-29 aircraft and forebody directional stability.

Forebody Pressure Distributions At $\alpha = 45°$, the forebody yawing moment at zero sideslip ($C_{n_{0,fb}}$) was nearly zero and the forebody directional stability was near maximum as shown in Figs. 7 and 9. Figure 10 shows the effects of sideslip on the forebody pressure distribution at x/l= 0.136. The outside surface of the cross section, as viewed from in front of the aircraft, is presented as $C_p = 0$. The curves represent the suction pressure coefficients ($-C_p$) about the surface for sideslip values of +3.3° (solid) and −3.8° (dashed). As shown in the figure, for positive sideslip, the suction pressure is greater on the windward side of the forebody near $\theta = 90°$ and less on the leeward side near $\theta = 270°$. Integration of these pressures results in a local yawing moment to the right (positive) for a positive angle of sideslip. The resulting $C_n\beta$ curve at $\alpha \approx 45°$ shows positive directional stability.

Effect of Mach Number

Pressure distributions were obtained on the forebody in windup turns at Mach numbers up to 0.6 as well as at lows speeds in 1-g stabilized flight. In Fig. 11, forebody pressure distributions at x/l = 0.026 are presented for an angle of attack from 25° to 40°. In this figure, the Mach number varies from 0.22 to 0.60 for nearly constant chord Reynolds numbers. At this location, the forebody strake is present. At $\alpha \approx 25°$, no significant Mach number effect was noted. However, at $\alpha \approx 30°$, 35°, and 40° a significant effect was noted. At $M = 0.60$, the suction peaks were reduced as compared to the lowest Mach number. In addition, the pressure distribution at $M = 0.60$ was no longer asymmetric as it had been at the lower Mach numbers.

Symbol	M	α	β	$Re_c \times 10^{-6}$
—•—	0.27	25.1	-0.2	7.0
—▪—	0.37	25.2	0.0	5.4
—▲—	0.49	24.9	-0.5	7.0
—◆—	0.61	25.6	0.4	8.3

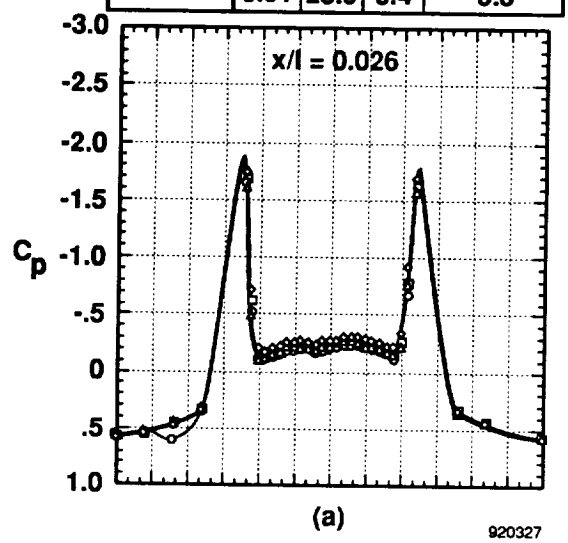

(a) $\alpha = 25°$.

Fig. 11 Effect of Mach number on forebody pressures, x/l = 0.026.

Symbol	α	β	C_n, (x/l = 0.136)
—○—	44.5°	+3.3°	.0062
---□---	45.1°	-3.8°	-.0041

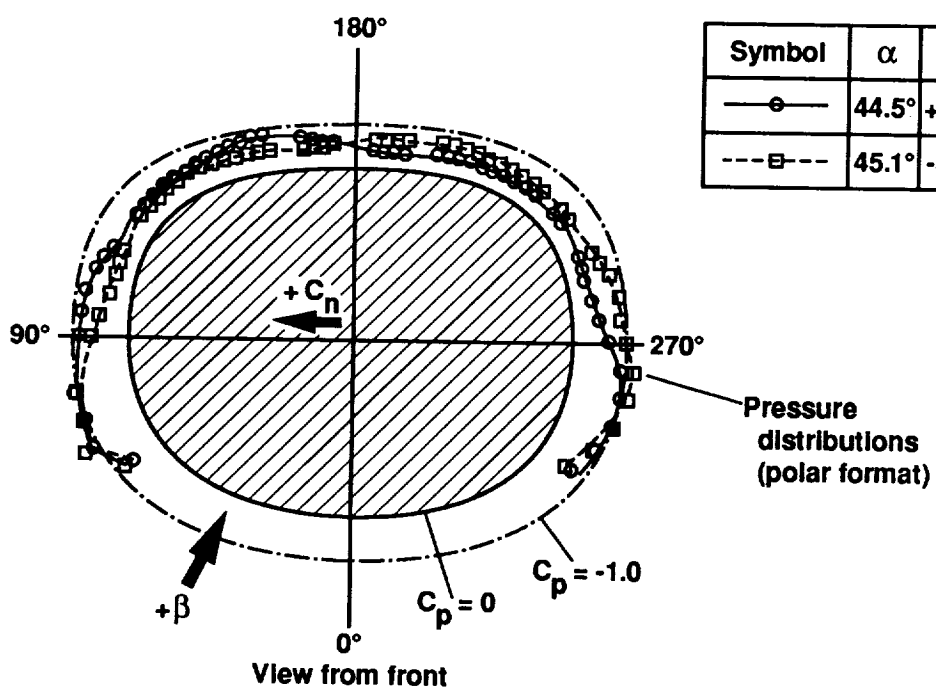

Fig. 10 Effect of angle of sideslip on forebody pressure distributions, $\alpha = 45°$.

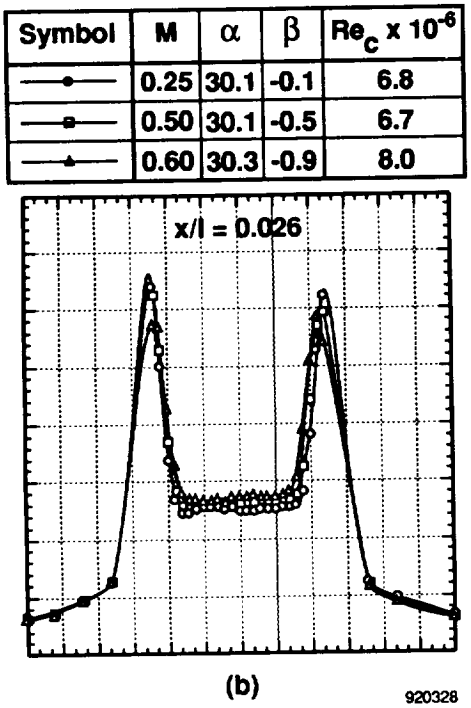

(b) $\alpha = 30°$.

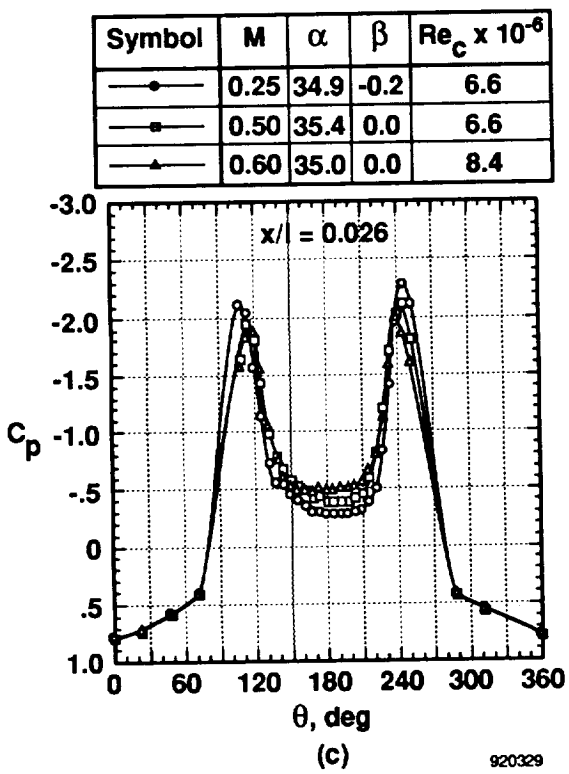

(c) $\alpha = 35°$.

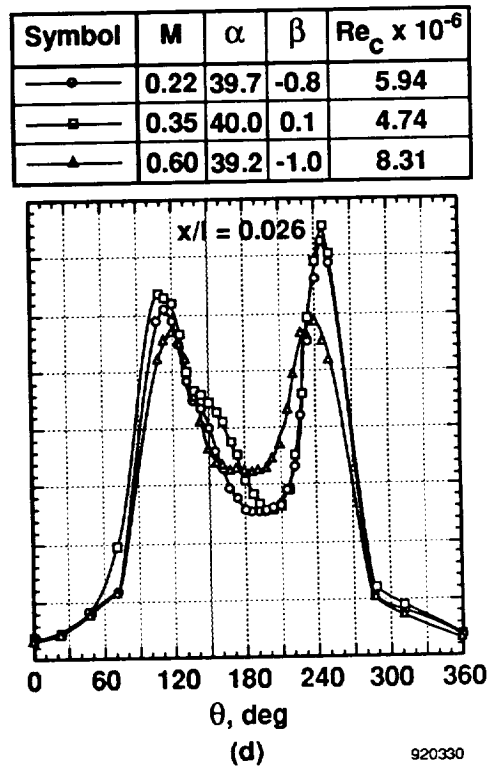

(d) $\alpha = 40°$.

Fig. 11 Concluded.

In Fig. 12, the forebody pressure distributions for one of the three aft stations, $x/l = 0.136$, are shown for an angle of attack from 25 to 40°. In contrast to the first station, the pressure distributions at the three aft stations did not show a significant Mach number effect. This shows a similar trend found on the F-18 HARV in which similar pressure distributions were taken on the forebody and on the leading-edge extensions. The F-18 forebody did not have a strake or noseboom and did not show a Mach number effect. However, on the leading-edge extensions where there was a sharp edge to induce flow separation at high angles of attack, a significant Mach number effect was noted.

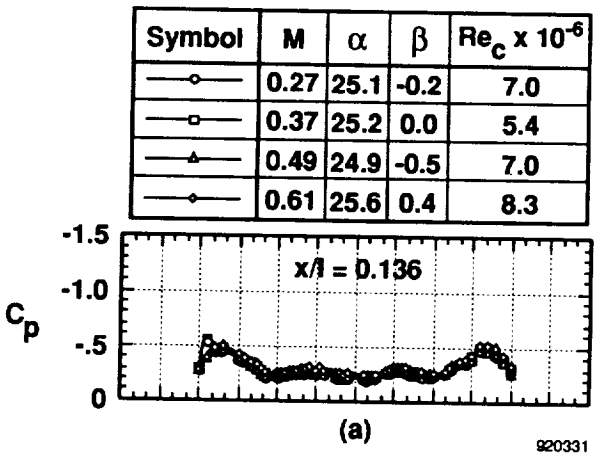

(a) $\alpha = 25°$.

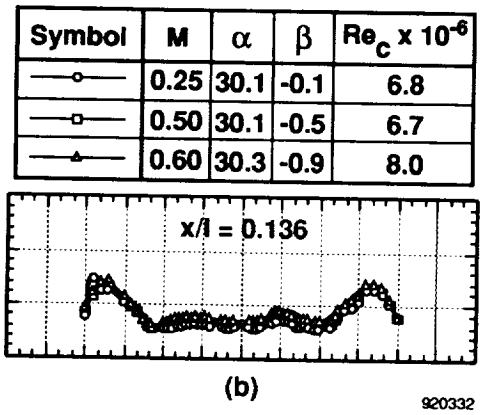

(b) $\alpha = 30°$.

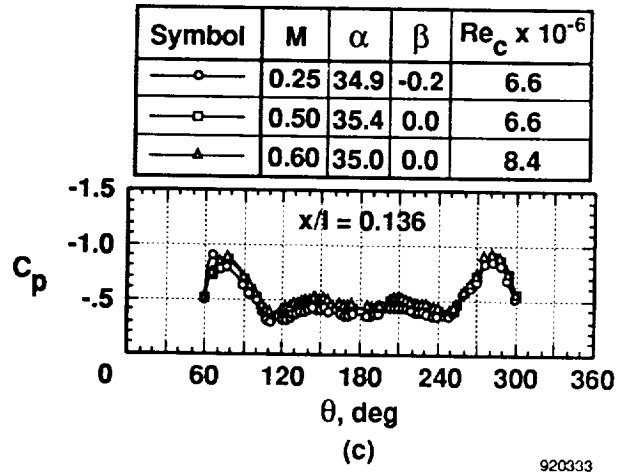

(c) $\alpha = 35°$.

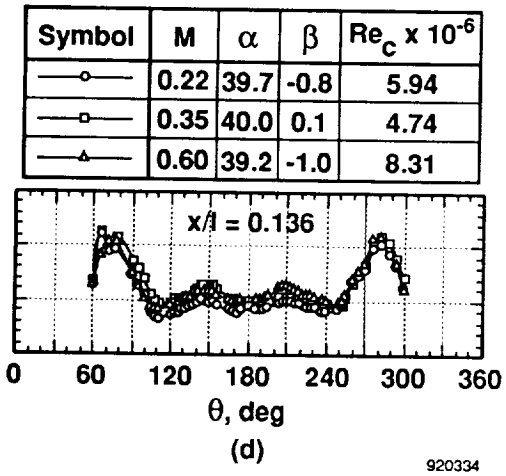

(d) $\alpha = 40°$.

Fig. 12 Effect of Mach number on forebody pressures, x/l = 0.136.

Effect of Reynolds Number

Only limited data were available to determine an effect of unit Reynolds number, i.e., data where the Mach number and angle of attack were nearly identical but the Reynolds number was varied. Forebody pressure distributions are presented in Fig. 13 for $\alpha \approx 25°$, $M \approx 0.50$ for $Re_c = 6.95$ and 14.05×10^6 ($Re_D = 3.19$ and 6.45×10^6, respectively) at x/l = 0.026 and 0.136. At all four fuselage stations, the pressure distributions were virtually identical except the two orifices on the lee side closest to the nose strake at x/l = 0.026 (Fig. 13(a)). In this case, only these two suction pressure coefficients were reduced at the higher Reynolds number conditions by $\Delta C_p \approx 0.5$. No effect of Reynolds number was noted at the aft station (Fig. 13(b)).

Symbol	α	β	M	$Re_c \times 10^{-6}$	$Re_D \times 10^{-6}$
—o—	24.9	-0.5	0.49	6.95	3.19
---□---	24.9	-0.9	0.53	14.05	6.45

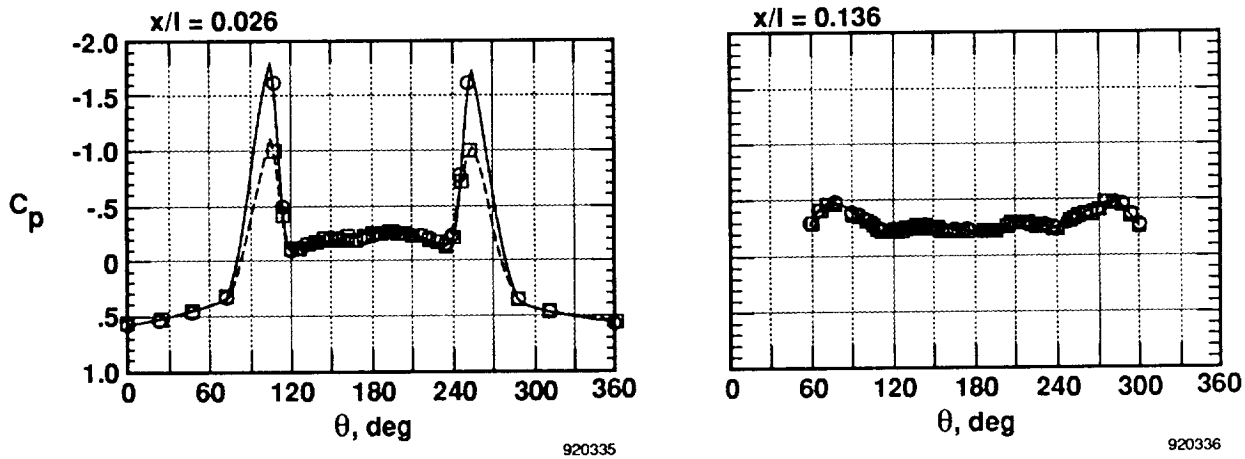

(a) x/l = 0.026.

(b) x/l = 0.136.

Fig. 13 Effect of Reynolds number on forebody pressure distributions, $\alpha = 25°$, $M = 0.50$.

Concluding Remarks

In-flight pressure distributions have been reported at angles of attack from 15 to 66° and at Mach numbers from 0.22 to 0.60 at four fuselage stations on the forebody of the X-29A aircraft. Forebody yawing moments were obtained from the integrated pressure distributions and the results were correlated with the overall aircraft yawing moments.

At angles of attack of 20° and higher, vortices shed from the nosestrake caused suction peaks in the pressure distribution that generally increased in magnitude with angle of attack. These suction peaks decreased in magnitude as one moved aft on the forebody. At angles of attack greater than or equal to 30°, the forebody pressure distribution became asymmetrical at the most forward station, x/l = 0.026. The pressure distributions remained nearly symmetrical until angles of attack from 50 to 55° for the aft stations. Between angles of attack of 59 to 66°, the asymmetry of the pressure distributions changed direction.

Yawing moments caused by the forebody did not become significant until an angle of attack of 50° or above and correlated well with the aircraft left yawing moment. The forebody yawing moments did not show a right yawing moment at an angle of attack of 45° as had been shown for the aircraft previously. However, the pressures at the aft station suggest that the canopy region could be causing this yawing moment. The forebody was shown to contribute to the directional stability of the aircraft at an angle of attack greater than or equal to 25°.

A Mach number effect was noted at an angle of attack of 30° or higher at the station where the nose strake was present. The suction peaks in the pressure distributions at this station and at the highest Mach number were reduced and much more symmetrical as compared to the lower Mach number pressure distributions.

References

[1]Trippensee, Gary, "X-29A High-Angle-of-Attack Testing," *Aerospace Engineering*, Oct. 1991.

[2]Moore, M. and D. Frei, "X-29 Forward Swept Wing Aerodynamic Overview," AIAA 83-1834, July 1983.

[3]Frei, Douglas, Melvin Garelick, Ronald Hendrickson, and Glenn Spacht, "Forward Swept Wing Study," AFFDL-TR-79-3151, Jan. 1980.

[4]Skow, A.M. and G.E. Erickson, "Modern Fighter Aircraft Design for High-Angle-of-Attack Maneuvering," AGARD Lecture Series No. 121, High Angle-of-Attack Aerodynamics, Mar. 1982, pp. 4-1 to 4-59.

[5]Grafton, S.B., W.P. Gilbert, M.A. Croom, and D.G. Murri, "High-Angle-of-Attack Characteristics of a Forward-Swept Wing Fighter Configuration," AIAA 82-1322, Aug. 1982.

[6]Murri, Daniel G., Luat T. Nguyen, and Sue B. Grafton, *Wind Tunnel Free-Flight Investigation of a Model of a Forward-Swept-Wing Fighter Configuration*, NASA TP-2230,1984.

[7]Fisher, David F., John H. Del Frate, and David M. Richwine, *In-Flight Flow Visualization Characteristics of the NASA F-18 High Alpha Research Vehicle at High Angles of Attack*, NASA TM-4193, 1990.

[8]Fisher, David F., Daniel W. Banks, and David M. Richwine, *F-18 High Alpha Research Vehicle Surface Pressures: Initial In-Flight Results and Correlation with Flow Visualization and Wind-Tunnel Data*, NASA TM-101724, 1990. Also published as AIAA 90-3018.

[9]Del Frate, John H. and Fanny A. Zuniga, "In-Flight Flow Field Analysis on the NASA F-18 High Alpha Research Vehicle With Comparisons to Ground Facility Data," AIAA 90-0231, 1990.

[10]Del Frate, John H. and John A. Saltzman, *Preliminary In-Flight Flow Visualization Results on the X-29 Aircraft at High Angles of Attack*, NASA CP-3137, Vol. 3, 1992, pp. 223–241.

[11]Del Frate, John H. and John A. Saltzman, "In-Flight Flow Visualization Results from the X-29 Aircraft at High Angles of Attack," AIAA 92-4102, Aug. 1992.

[12]Fisher, David F., David M. Richwine, and Stephen F. Landers, *Preliminary Results of Forebody Pressure Measurements on the X-29A Aircraft at High Angles of Attack*, NASA CP-3137, Vol. 3, 1992, pp. 243–259.

[13]Grafton, Sue B., Joseph R. Chambers, and Paul L. Coe, Jr., *Wind-Tunnel Free-Flight Investigation of a Model of a Spin-Resistant Fighter Configuration*, NASA TN D-7716,1974.

[14]Whitmore, Stephen A., Timothy R. Moes, and Terry J. Larson, *Preliminary Results From a Subsonic High Angle-of-Attack Flush Airdata Sensing (HI-FADS) System: Design, Calibration, and Flight Test Evaluation*, NASA TM-101713, 1990.

[15]Moes, Timothy R. and Stephen A. Whitmore, *A Preliminary Look at Techniques Used to Obtain Airdata From Flight at High Angles of Attack*, NASA TM-101729, 1990.

[16]Rajczewski, David M., "X-29 High Angle-of-Attack Flight Test: Air Data Comparisons of an Inertial Navigation System and Noseboom Probe," Society of Flight Test Engineers (SFTE) 21st Annual Symposium, Garden Grove, CA, Aug. 1990.

[17]Pellicano, Paul, Joseph Krumenacker, and David Vanhoy, "X-29 High Angle-of-Attack Flight Test Procedures, Results, and Lessons Learned," Society of Flight Test Engineers (SFTE) 21st Annual Symposium, Garden Grove, CA, Aug. 1990.

[18]Lamont, P.J., "Pressure Measurements on an Ogive-Cylinder at High Angles of Attack with Laminar, Transitional, or Turbulent Separation," AIAA 80-1556, Jan. 1980.

[19]Keener, Earl R., Gary T. Chapman, Lee Cohen, and Jamshid Taleghani, *Side Forces on a Tangent Ogive Forebody with a Fineness Ratio of 3.5 at High Angles of Attack and Mach Numbers from 0.1 to 0.7*, NASA TM X-3437, 1977.

[20]Keener, Earl R., Gary T. Chapman, Lee Cohen, and Jamshid Taleghani, *Side Forces on Forebodies at High Angles of Attack and Mach Numbers From 0.1 to 0.7: Two Tangent Ogives, Paraboloid and Cone*, NASA TM X-3438, 1977.

[21]Webster, Fredrick R. and Dana Purifoy, "X-29 High Angle-of-Attack Flying Qualities," AFFTC-TR-91-15, July 1991.

[22]Hunt, B.L., "Asymmetric Vortex Forces and Wakes on Slender Bodies," AIAA 82-1336, Aug. 1982.

[23]Klein, Vladislav, Brent R. Cobleigh, and Keith D. Noderer, *Lateral Aerodynamic Parameters of the X-29 Aircraft Estimated From Flight Data at Moderate to High Angles of Attack*, NASA TM-104155, 1991.

REPORT DOCUMENTATION PAGE

Form Approved
OMB No. 0704-0188

Public reporting burden for this collection of information is estimated to average 1 hour per response, including the time for reviewing instructions, searching existing data sources, gathering and maintaining the data needed, and completing and reviewing the collection of information. Send comments regarding this burden estimate or any other aspect of this collection of information, including suggestions for reducing this burden, to Washington Headquarters Services, Directorate for Information Operations and Reports, 1215 Jefferson Davis Highway, Suite 1204, Arlington, VA 22202-4302, and to the Office of Management and Budget, Paperwork Reduction Project (0704-0188), Washington, DC 20503.

1. AGENCY USE ONLY *(Leave blank)*	2. REPORT DATE	3. REPORT TYPE AND DATES COVERED
	November 1992	Technical Memorandum

4. TITLE AND SUBTITLE

Correlation of Forebody Pressures and Aircraft Yawing Moments on the X-29A Aircraft at High Angles of Attack

5. FUNDING NUMBERS

RTOP 533-02-38

6. AUTHOR(S)

David F. Fisher, David M. Richwine, and Stephen Landers

7. PERFORMING ORGANIZATION NAME(S) AND ADDRESS(ES)

NASA Dryden Flight Research Facility
P.O. Box 273
Edwards, California 93523-0273

8. PERFORMING ORGANIZATION REPORT NUMBER

H-1851

9. SPONSORING/MONITORING AGENCY NAME(S) AND ADDRESS(ES)

National Aeronautics and Space Administration
Washington, DC 20546-0001

10. SPONSORING/MONITORING AGENCY REPORT NUMBER

NASA TM-4417

11. SUPPLEMENTARY NOTES

Fisher: Dryden Flight Research Facility, Edwards, CA; Richwine and Landers: PRC Inc., Edwards, CA.
Presented as AIAA paper 92-4105 at the AIAA Flight Test Conference, Hilton Head, SC, August 24–26, 1992.

12a. DISTRIBUTION/AVAILABILITY STATEMENT

Unclassified — Unlimited
Subject Category 02

12b. DISTRIBUTION CODE

13. ABSTRACT *(Maximum 200 words)*

In-flight pressure distributions at four fuselage stations on the forebody of the X-29A aircraft have been reported at angles of attack from 15 to 66° and at Mach numbers from 0.22 to 0.60. At angles of attack of 20° and higher, vortices shed from the nose strake caused suction peaks in the pressure distributions that generally increased in magnitude with angle of attack. Above 30°-angle of attack, the forebody pressure distributions became asymmetrical at the most forward station, while they remained nearly symmetrical until 50- to 55°-angle of attack for the aft stations. Between 59- to 66°-angle of attack, the asymmetry of the pressure distributions changed direction. Yawing moments for the forebody alone were obtained by integrating the forebody pressure distributions. At 45°-angle of attack, the aircraft yaws to the right and at 50° and higher, the aircraft yaws to the left. The forebody yawing moments correlated well with the aircraft left yawing moment at an angle of attack of 50° or higher. At a 45°-angle of attack, the forebody yawing moments did not correlate well with the aircraft yawing moment, but it is suggested that this was due to asymmetric pressures on the cockpit region of the fuselage which was not instrumented. The forebody was also shown to provide a positive component of directional stability of the aircraft at angles of attack of 25° or higher. A Mach number effect was noted at angles of attack of 30° or higher at the station where the nose strake was present. At this station, the suction peaks in the pressure distributions at the highest Mach number were reduced and much more symmetrical as compared to the lower Mach number pressure distributions.

14. SUBJECT TERMS

Flight test, Forebody, High-angle-of-attack, Pressure distribution, Vortex flow, X-29

15. NUMBER OF PAGES

16

16. PRICE CODE

A03

17. SECURITY CLASSIFICATION OF REPORT	18. SECURITY CLASSIFICATION OF THIS PAGE	19. SECURITY CLASSIFICATION OF ABSTRACT	20. LIMITATION OF ABSTRACT
Unclassified	Unclassified	Unclassified	Unlimited